Optical Materials 137 (2023) 113543

Contents lists available at ScienceDirect

Optical Materials

journal homepage: www.elsevier.com/locate/optmat

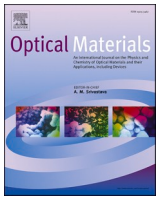

Research Article

(INVITED)Mid-infrared photoluminescence in Ce^{3+} doped selenide-chalcogenide glass and fiber

Joel J. Nunes [a], Richard W. Crane [a], Zhuoqi Tang [a], Łukasz Sójka [b], Nikolaos Kalfagiannis [c], David Furniss [a], Mark C. Farries [a], Trevor M. Benson [a], Slawomir Sujecki [b], Angela B. Seddon [a,*]

[a] Mid-Infrared Photonics Group, George Green Institute for Electromagnetics Research, Faculty of Engineering, University of Nottingham, University Park, Nottingham, NG7 2RD, UK

[b] Department of Telecommunications and Teleinformatics, Faculty of Electronics, Wroclaw University of Science and Technology, Wybrzeze Wyspianskiego 27, 50-370, Wroclaw, Poland

[c] School of Science and Technology, Department of Physics and Mathematics, Nottingham Trent University, Clifton Campus, Nottingham, NG11 8NS, UK

A B S T R A C T

We provide measurements to support our earlier report of continuous wave fiber lasing in a small core Ce^{3+}-doped selenide chalcogenide SIF (*step index fiber*) of core: Ge-As-Ga-Se chalcogenide glass, doped with 500 ppmw (*parts-per-million by weight*) of cerium (III). In-band pumping of Ce^{3+} in fiber, bulk glass and ground glass geometries, at 4.15 μm wavelength, gives MIR (*mid-infrared*) photoluminescence spanning 3.40–5.80 μm wavelength, corresponding to the $^2F_{5/2} \leftarrow {}^2F_{7/2}$ electronic emission transition due to Ce^{3+}. Room temperature emission and MIR absorption spectra together enable interpretation of the manifold energies of the first excited state and there is potential for occupied Stark levels in the ground state at room temperature. Both 'τ_{rad}' (PL lifetime) and 't_{rise}' (rise-time through 10% to 90% of maximum PL intensity) are determined: for ground glass at 4.60 μm wavelength, the best decay fit comprises a primary, and perhaps secondary, lifetime for ground glass of 3.5 ms, and 1.2 ms, and PL rise time of 3.9 ms.

1. Introduction

The photoluminescent properties of trivalent lanthanide dopants in chalcogenide glass hosts are of significant interest due to their potential use as MIR (*mid-infrared*) light sources (see for instance [1,2]). In 2021 [3], we reported for the first time CW (*continuous wave*) MIR fiber lasing beyond 5 room temperature. This was achieved in a 500 ppmw ((*parts-per-million by weight*) Ce-foil doped, selenide-chalcogenide glass (Ge-As-Ga-Se), SIF (*step index fiber*), of 9 μm diameter core, 64 mm long, with NA (*numerical aperture*) 0.48 at the lasing wavelengths. CW lasing was observed at 5.14 μm, 5.17 μm, and 5.28 μm, corresponding to the $^2F_{5/2} \leftarrow {}^2F_{7/2}$ emission of the Ce^{3+} ion, on in-band pumping using a 4.15 μm QCL (*quantum cascade laser*) and the lasing threshold was 86 mW pump power [3]. In the same year, bulk glass lasing was also reported of Ce^{3+} in Ge-Sb-Ga-Se pumped using a pulsed Fe^{2+}:ZnSe laser at 4.1 μm, giving 35 mJ maximum output energy at 5.2 μm, with a lasing threshold of about 60 mJ, slope efficiency of 21% and tuning range of 4.5–5.6 μm [4].

The work presented here was mainly carried out prior to achieving fibre lasing [3] and is a more detailed investigation of photoluminescence (PL) in the Ce^{3+}doped [5,6] selenide chalcogenide glass system.

Traditionally, the luminescent properties of Ce compounds have concentrated on their 5 d → 4f electronic transitions, occurring in the ultraviolet and visible spectral regions [7–11] However, here we focus on the 4f ⇌ 4f intra-electronic transitions whose energy changes occur in the MIR spectral region. The 4f energy level diagram (see Fig. 1(c)) of Ce^{3+} comprises the $^2F_{5/2}$ ground state and one excited state manifold: $^2F_{7/2}$, ruling out ESA (*excited state absorption*). However, the excited state manifold is exceptionally broad. In other work involving Ce^{3+}-doped oxide hosts, it has been suggested that there is existence, and occupancy at room temperature, of an upper second Stark level in the ground state, named as a 'hot transition' [7].

The selenide chalcogenide host glass provides a low phonon energy, MIR transparent host for the Ce^{3+} dopant, which is amenable to fiber drawing. The two-level f-electronic structure of the Ce^{3+} cation precludes any MIR inter-state excited state absorption, this coupled with an inherently small quantum defect afforded by in-band pumping, makes Ce^{3+} doped chalcogenide glass an excellent candidate for implementing efficient, relatively compact, and robust MIR light sources, such as the MIR fiber laser [3]. These narrow-band MIR light sources are attractive for applications in chemical and biochemical molecular sensing as

* Corresponding author.
E-mail address: angela.seddon@nottingham.ac.uk (A.B. Seddon).

https://doi.org/10.1016/j.optmat.2023.113543
Received 21 January 2023; Accepted 30 January 2023
Available online 27 February 2023

numerous molecular species exhibit their fundamental spectroscopic vibrational absorption bands in the MIR spectral region [12–15]. In addition, long wavelength narrow-band MIR fibre lasers present excellent beam quality, potentially suitable for providing new wavelengths for medical laser surgery and polymer machining. Finally, MIR fibre lasers have potential for pumping supercontinuum MIR fibre light sources for all-fibre, compact broadband molecular sensing.

In this paper, we report on the synthesis and characterization, of cerium-foil doped Ge-As-Ga-Se chalcogenide glass. Section 2 describes the experimental methods employed in the fabrication, and characterization, of Ce-foil doped bulk and ground glass, unstructured fiber and SIF (*step-index fiber*), all having the same nominal host glass composition (originating from the same glass melt), and presents the corresponding results of fiber properties, MIR Ce^{3+} absorption, and PL emission spectra, lifetime and rise time measurements. In Section 3 the results are discussed.

In our work here, and in the fibre laser reported in [3], we assume that the Ce dopant once incorporated in the chalcogenide host glass is in the Ce^{3+} oxidation state. However, we cannot exclude the possibility of the tetravalent state: Ce^{4+} [5,6] which comprises an inner electronic configuration of [Xe], with no available '4f' electrons for 4f ⇌ 4f intra-electronic transitions and therefore no electronic mechanism to produce MIR absorption or PL. We are pursuing further work to assess any co-existence of Ce^{3+}/Ce^{4+} ions in selenide-chalcogenide glass networks.

2. Methods and experimental results

Section 2.1 describes the synthesis and fabrication of Ce-foil doped bulk chalcogenide glass, unstructured fiber, ground glass and SIF, and the SIF cladding glass. Section 2.2 describes the methodology and presents the results of measuring optical loss of the unstructured fibre,

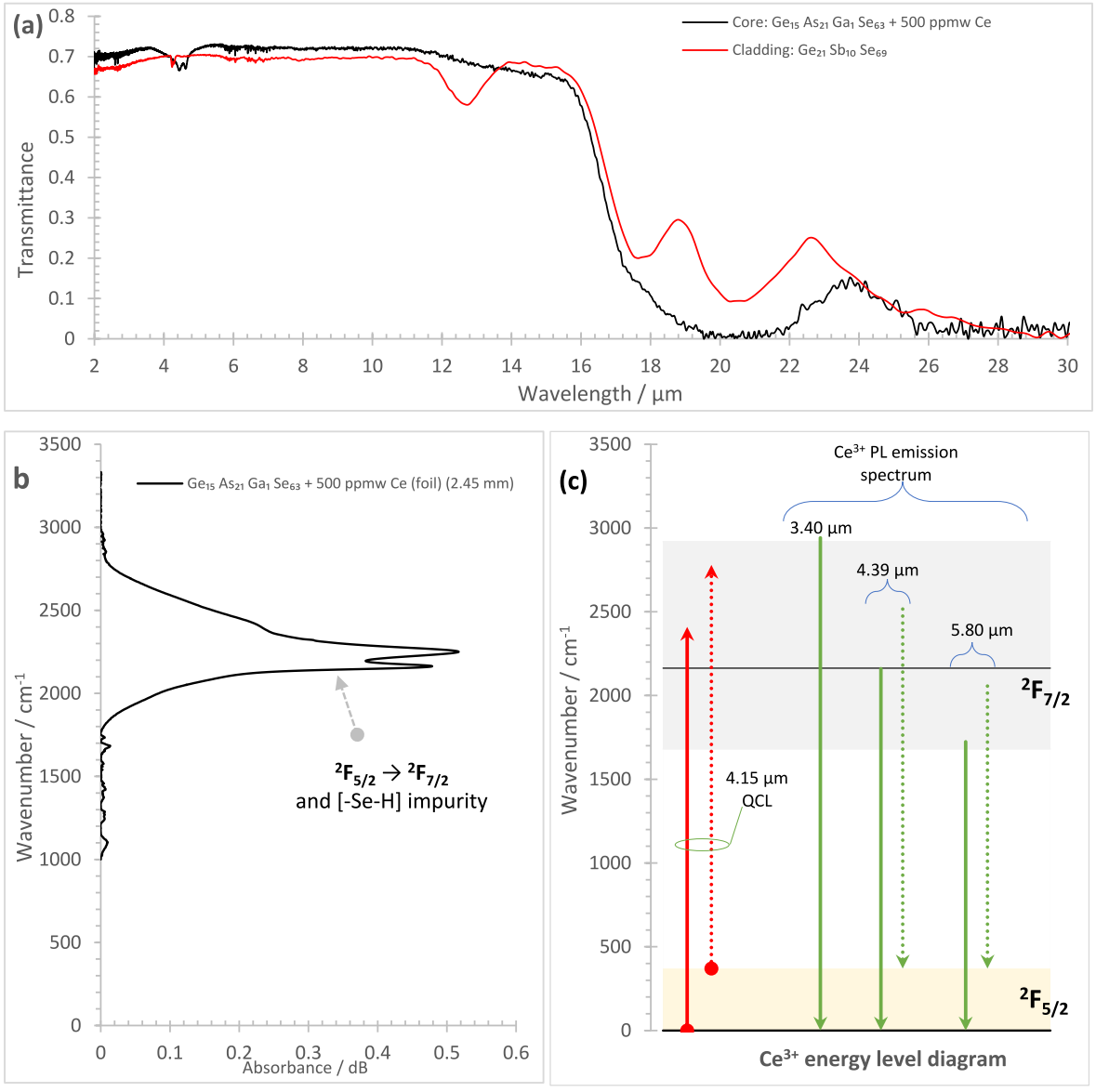

Fig. 1. (**a**) The transmittance spectrum of bulk glass of nominal as-batched composition $Ge_{15.0}$ $As_{21.0}$ $Ga_{1.0}$ $Se_{63.0}$ at. % + 500 ppmw Ce foil (code: **M259REZQT**) of 2.45 mm optical pathlength and of bulk glass of nominal as-batched composition: $Ge_{21.0}$ $Sb_{10.0}$ $Se_{69.0}$ at. % (code: **M287RC**) of 3 mm optical pathlength, (**b**) the room temperature MIR absorption spectrum for the nominal as-batched composition: $Ge_{15.0}$ $As_{21.0}$ $Ga_{1.0}$ $Se_{63.0}$ atomic % + 500 ppmw Ce foil doped bulk sample of 2.45 mm minimum optical pathlength with the host glass baseline numerically removed, and (**c**) the corresponding Ce^{3+} electronic energy level diagram overlaid with the 4.15 µm excitation wavelength from the QCL source and Ce^{3+} PL emission wavelengths. Note: the arrow lengths are accurately scaled to energy, and the gray box and amber box denote the extent of the splitting of the Stark states in the $^2F_{7/2}$ and $^2F_{5/2}$ manifolds, respectively.

refractive index dispersion of the bulk glasses, and calculated SIF NA, and PL emission measurements performed on Ce-foil doped unstructured fiber, bulk glass, SIF, and ground glass samples.

2.1. Melting of core and cladding glasses, extrusion, and fiber-drawing

Two chalcogenide glass compositions *viz.*: Ce-foil doped Ge-As-Ga-Se and undoped Ge-Sb-Se, were synthesized in rod form using the 'Melt-Quench' method (see Section 2.1.1). The Ce-foil doped Ge-As-Ga-Se rod was drawn to unstructured fiber; part of this unstructured fiber was ground for luminescence studies. The Ce-foil doped Ge-As-Ga-Se synthesized rod was also cane-drawn; the undoped Ge-Sb-Se glass rod was extruded to form a tube, into which the Ce-foil doped cane was inserted and the cane-in-tube preform was drawn to SIF. Thus, the undoped Ge-Sb-Se glass was used solely as the optical cladding in the SIF.

2.1.1. Bulk glass syntheses

To prepare the Ce-foil doped Ge-As-Ga-Se glass, firstly volatile oxide impurities were removed from the As and Se elemental chemical precursors: arsenic 'As' (*Furakawa Denshi, 7N5 purity*) was baked at 310 °C/1.5 h, and Se (*Materion, 5 N purity*) at 260 °C/2 h, both under 10^{-3} Pa. As, Se, Ge (*Materion, 5 N purity*), and Ga (*Alfa Aesar, 7N5 purity*) were then batched into a silica glass ampoule (*Multilab:* < 5 ppm *OH, ID/OD (internal diameter/external) diameter of* 10 mm/14 mm*, prior air-baked, then vacuum-baked, both at 1000 °C/6 h*), inside a MBraun glovebox (*N_2:* < *0.*6 ppm *H_2O and* < *0.*3 ppm *O_2*). This ampoule and contents were vacuum-sealed at 10^{-3} Pa. This melt ampoule was then heated at 850 °C/12 h in a rocking furnace for melt homogenization; then cooled to, and held at, 700 °C/2 h while still in the melt furnace in a stationary vertical hold for refining and fining. The glass melt, *in situ* inside the ampoule, was quenched and then annealed for 1.5 h at 243 °C, before cooling with the furnace to ambient. The ampoule was returned to the glovebox, opened and 500 ppmw Ce foil (*Alfa Aesar, 3 N purity*) was added. The ampoule was then re-sealed under vacuum, re-heated at 850 °C/2 h in a rocking furnace and then cooled for refining/fining, quenched and annealed as before. The resulting 10 mm diameter glass rod was, as-batched, 500 ppmw Ce-foil doped $Ge_{15.0}$ $As_{21.0}$ $Ga_{1.0}$ $Se_{63.0}$ at. % (*code: M259REZQT*).

For the Ge-Sb-Se glass melt, the purity and prior purification treatment of the elemental precursors: Ge and Se were as above, while antimony 'Sb' (*Materion, 5 N purity*) was prior baked at 570 °C/3 h under 10^{-3} Pa to drive off oxide. These purified elemental precursors were batched, and vacuum sealed in a silica glass ampoule (*Multilab:* < 5 ppm *OH, ID/OD of 26.*5 mm/30 mm*, prior air-baked, then vacuum-baked, both at 1000 °C/6 h*), heated at 900 °C/12 h in a rocking furnace, cooled for refining and fining, then quenched and annealed 227 °C/1 h. The resulting 26 mm diameter glass rod was, as-batched, $Ge_{21.0}$ $Sb_{10.0}$ $Se_{69.0}$ at. % (*code:* ***M*287RC**).

2.1.2. Extrusion of cladding glass-melt

Glass-melt extrusion was performed under nitrogen using an in-house made hydraulic extruder, fitted with an electric resistance furnace. The undoped $Ge_{21.0}$ $Sb_{10.0}$ $Se_{69.0}$ at. % glass rod (*code:* ***M*287RC**), prepared as in Section 2.1.1, was extruded to form a cladding tube (code: **E093**) with an ID/OD (*inner diameter/outer diameter*) of ~1 mm/~10 mm, as further described in [16,17].

2.1.3. Drawing of unstructured fibre and cane, and SIF (step-index fiber)

Fiber- and cane-drawing were performed, on a modified Heathway fiber-draw tower fitted with a radio frequency furnace, housed in a class-10,000 clean room, of the Ce-foil doped $Ge_{15.0}$ $As_{21.0}$ $Ga_{1.0}$ $Se_{63.0}$ at. % glass rod (*code: M259REZQT*, prepared as Section 2.1.1) to make the unstructured fiber (code: ***F109REZQT(RC&JN)***) OD ~200 μm, and unstructured cane OD ~600 μm (code: ***F109REZQT(RC&JN)*-cane**).

Small core fibre fabrication methods for heavy metal oxide and chalcogenide glasses have been reported [18–20]. Here, SIF was fabricated as in [21], thus, the Ce-foil doped Ge-As-Ga-Se unstructured cane (*code:* ***F109REZQT(RC&JN)*-cane**) was inserted inside the orifice of the extruded, cladding Ge-Sb-Se glass tube (code: **E093**), Section 2.1.2) and this cane-in-tube preform was drawn to the SIF (*code:* ***F*130RERC**). Drawing was done under vacuum, to obviate unwanted gaps at the SIF core/cladding interface.

2.2. Bulk glass and fiber characterization and results

The Ce-foil doped Ge-As-Ga-Se glass rod (*code:* ***M259REZQT***), synthesized by the 'Melt-Quench' method (Section 2.1.1) was sawn orthogonally to the rod axis to form a disc, and the disc faces were ground and polished ready for absorption spectroscopy (Sections 2.2.1 and 2.2.5), and refractive index (Section 2.2.2) measurements. Fiber attenuation was measured of the Ce-foil doped Ge-As-Ga-Se unstructured fiber (code: ***F109REZQT(RC&JN)***, Section 2.2.3), drawn from the as-annealed Ce-foil doped glass rod (*code:* ***M259REZQT***, Section 2.1.1). PL emission spectroscopy (Section 2.2.5), PL lifetime and rise-time were measured on different geometry glass samples that had <u>*all*</u> originated from synthesized Ce-foil doped Ge-As-Ga-Se glass rod *(code:* ***M259REZQT)***, viz.: *bulk* glass, unstructured fiber, in its fiber and ground form, and SIF with the Ce-foil doped Ge-As-Ga-Se glass as its core.

2.2.1. FtIR (fourier transform infrared)

(i) Method

Room temperature FtIR (Fourier transform infrared) absorption spectra were collected on disc samples sliced from the as-annealed Ce-foil doped Ge-As-Ge-Se glass rod (*code:* ***M259REZQT***, Section 2.1.1) and the undoped, as-annealed Ge-Sb-Se glass rod (*code:* ***M*287RC**, Section 2.1.1); the disc samples were ground to have parallel, opposite faces, and polished to a 1-μm surface finish to give an optical pathlength of 2.45 mm (former) and 3 mm (latter). Further details are in [22].

(ii) Results

Fig. 1(a) shows the room temperature absorption spectra for the 500 ppmw Ce foil doped $Ge_{15.0}$ $As_{21.0}$ $Ga_{1.0}$ $Se_{63.0}$ at. % (*code:* ***M259REZQT***), and $Ge_{21.0}$ $Sb_{10.0}$ $Se_{69.0}$ at. % (*code:* ***M*287RC**) bulk samples. Fig. 1(b) shows the same room temperature Ce^{3+} MIR absorption spectrum as in Fig. 1(a) but with the host glass baseline contributions numerically removed; this spectrum was used to infer the corresponding Ce^{3+} energy level diagram shown in Fig. 1(c), with upper and lower limits of the $^2F_{7/2}$ manifold shaded in gray.

Considering Fig. 1(a) and (b), the $^2F_{5/2} \rightarrow {}^2F_{7/2}$ ground state absorption is manifested spanning 3.33–5.56 μm *(3000*-1800 cm^{-1}), apparently centered at 4.63 μm (2160 cm^{-1}). This wide absorption band of Ce^{3+} overlaps, and is resonant with, extrinsic absorption of [-Se-H] impurity in the glass host [23–26]. For Pr^{3+}-doped Ge-As-Ga-Se glasses, an apparent peak absorption of Pr^{3+} at 4.6 μm (2174 cm^{-1}) was found to be an artefact when the absorption band was modelled and deconvoluted into the electronic absorption of Pr^{3+} and vibrational absorption of [-Se-H (see Fig. 6 in [25]). From Fig. 1(b), the second maximum peak absorption of Ce^{3+} is at 4.39 (2280 cm^{-1}) μm and is more likely to be real than the apparent peak at 4.6 μm and hence is included in the Ce^{3+} energy level diagram of Fig. 1(c) [27,28]. Importantly, from Fig. 1(b), the upper $^2F_{7/2}$ energy level can be inferred to exhibit extensive, non-degenerate, Stark splitting and spans *ca.* 1130 cm^{-1}, which has also been typically found for Ce^{3+} in oxide hosts [11,12]. In oxide hosts, it has been suggested that there is some occupancy of upper Stark levels in the $^2F_{5/2}$ ground state at room temperature [7]. Thus, the $^2F_{5/2}$ ground state, inclusive of its Stark splitting is shown in Fig. 1(c). However, we found no emission at ~7.7 μm wavelength, which would be the predicted emission from the lowest Stark level of the excited state to the uppermost level of the ground state. Thus, there remains a question

about the degeneracy of Stark levels in the ground state for Ce^{3+} in these very low phonon energy hosts.

The potential presence of the Ce^{4+} valence state [10,11] and underlying [-Se-H] impurity vibrational absorption confounds accurate measurement of the Ce^{3+} absorption cross-section here.

2.2.2. Refractive index dispersion

(i) Method

MIR refractive indices were collected on disc samples sliced from the as-annealed Ce-foil doped Ge-As-Ge-Se glass rod (*code:* ***M259REZQT***, Section 2.1.1) and the undoped, as-annealed Ge-Sb-Se glass rod (*code:* ***M287RC***, Section 2.1.1); the disc samples were ground to have parallel, opposite faces; one face was polished to a 1-μm surface finish and the opposite face roughened using 120 grit paper to eliminate secondary specular reflections during the measurements. Variable angle spectrometric ellipsometry (*Woollam IR-VASE Mark II*) was utilized to measure samples at angles of 55°, 65° and 75°, and the results modelled assuming an oxidized, lower index layer at the glass surface.

(ii) Results

Fig. 2 showed the refractive index dispersion determined of the 500 ppmw Ce-foil doped $Ge_{15.0}$ $As_{21.0}$ $Ga_{1.0}$ $Se_{63.0}$ at. % (*code: M259REZQT*) and $Ge_{21.0}$ $Sb_{10.0}$ $Se_{69.0}$ at. % (*code: M2*87RC). From Fig. 2, at 3 μm wavelength, and 10 μm wavelength, the refractive indices are 2.568 and 2.558 for the cerium-doped composition and 2.526 and 2.508 for the none-cerium doped glass, respectively. The measured refractive index dispersion enables calculation of the NA of the SIF comprising a core// cladding of 500 ppmw Ce-foil doped $Ge_{15.0}$ $As_{21.0}$ $Ga_{1.0}$ $Se_{63.0}$ at. % (*code: M259REZQT*)//$Ge_{21.0}$ $Sb_{10.0}$ $Se_{69.0}$ at. % (*code:* ***M287RC***), which was 0.465 at 3 μm wavelength and 0.485 at 10 μm wavelength, respectively. However, the actual NA of the SIF will differ due to its different thermal history, of fast cooling after fiber drawing, from the as-annealed glasses whose refractive index dispersions were actually measured.

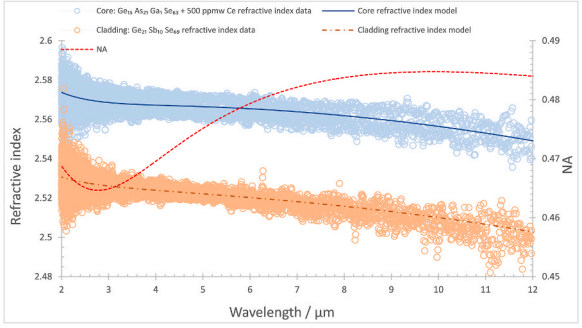

Fig. 2. Refractive index dispersion of the as-annealed 500 ppmw Ce-foil doped $Ge_{15.0}$ $As_{21.0}$ $Ga_{1.0}$ $Se_{63.0}$ at. % and the as-annealed $Ge_{21.0}$ $Sb_{10.0}$ $Se_{69.0}$ at. % bulk glasses, measured using variable angle spectrometric ellipsometry, and the calculated NA of the SIF comprising core/cladding = 500 ppmw Ce-foil doped $Ge_{15.0}$ $As_{21.0}$ $Ga_{1.0}$ $Se_{63.0}$ at. %/$Ge_{21.0}$ $Sb_{10.0}$ $Se_{69.0}$ at. %. Note the glasses comprising the SIF are from the same glasses melts as those bulk samples measured but the SIF has a different thermal history and was fast quenched during drawing (Reproduced from [3].).

2.2.3. Optical attenuation of unstructured fiber

MIR attenuation of the 500 ppmw Ce-foil doped $Ge_{15.0}$ $As_{21.0}$ $Ga_{1.0}$ $Se_{63.0}$ at. % unstructured fiber (Section 2.1.3) was measured using the 'cut-back' method as in [22]. Fig. 3 shows the optical attenuation spectrum for 2.75 m of the unstructured fiber, of 246 μm diameter. From Fig. 3, the minimum optical loss was 2.23 dB/m at 6.90 μm wavelength. The SIF, prepared as in Section 2.1.3, would have exhibited at least the optical loss shown in Fig. 3; more loss may have been incurred during the extra thermal processing in going from the cane (drawn at the same time and from the same preform as the unstructured fibre and hence likely to exhibit a similar loss characteristic to that of the unstructured fibre) to the SIF *via* cane-in-tube fibre-drawing.

2.2.4. Composition and structure of the SIF (step-index fiber)

Imaging and compositional analysis of a freshly cleaved SIF sample, fabricated as in Section 2.1.3, was carried out using a JEOL 6490LV SEM (*scanning electron microscopy*) fitted with an X-Max 80 Oxford Instruments EDX (*energy dispersive X-ray spectroscopy*) detector (± *0.5 atomic % accuracy for elements heavier than oxygen*).

The SEM-EDX evaluation revealed a measured core host glass composition of $Ge_{16.2}$ $As_{20.0}$ $Ga_{0.9}$ $Se_{62.9}$ ± 0.5 at.% (cf. *As batched:* $Ge_{15.0}$ $As_{21.0}$ $Ga_{1.0}$ $Se_{63.0}$ *at. %*); the cerium dopant level was too small to be measured using SEM EDX. The SEM EDX measured cladding glass composition was $Ge_{21.5}$ $Sb_{11.2}$ $Se_{67.3}$ ± 0.5 at *%*, (cf. *As-batched:* $Ge_{21.0}$ $Sb_{10.0}$ $Se_{69.0}$ *at. %*) indicating selenium loss during processing. Fig. 4(a) and (b) depict SEM images of a cleaved SIF sample with 19 μm diameter core - revealing that the core was circular and concentrically centered within the cladding.

2.2.5. Photoluminescence emission spectra, PL lifetimes and PL rise-times

(i) Method

The PL emission spectra, lifetime and rise time of the Ce-doped Ge-As-Ga-Se as-annealed bulk glass, unstructured fibre, powdered unstructured fibre and SIF (prepared as in Section 2.1), were investigated

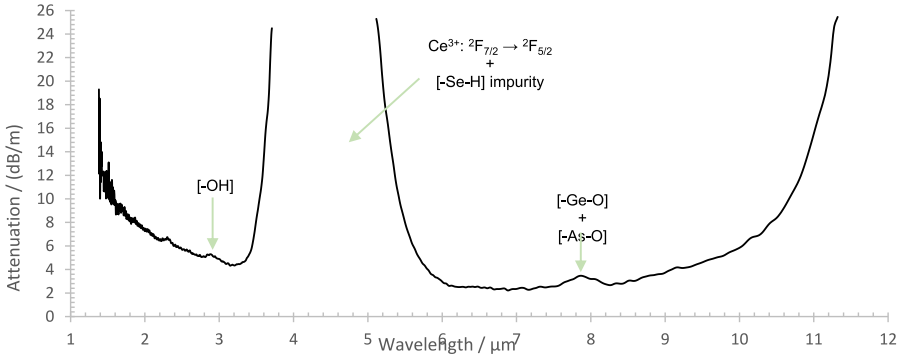

Fig. 3. MIR optical loss spectrum of nominal as-batched $Ge_{15.0}$ $As_{21.0}$ $Ga_{1.0}$ $Se_{63.0}$ at. % + 500 ppmw Ce foil doped unstructured glass fiber, 2.75 m long and 246 μm diameter. Ce^{3+} ground-state electronic absorption and extrinsic vibrational absorption loss due to the presence of unwanted, host glass hydride, oxide and hydroxide impurities are identified. A minimum loss of 2.23 dB/m occurs at 6.90 μm (Reproduced from [3].).

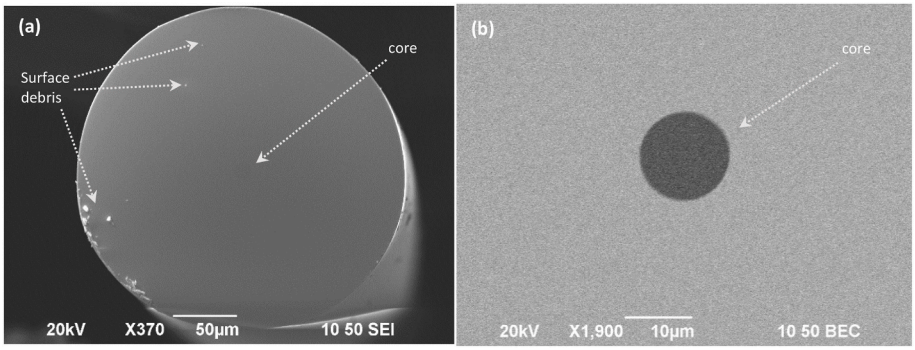

Fig. 4. SEM images of cleaved end of SIF (step index fiber) sample of core//cladding = nominal as-batched 500 ppmw Ce-foil doped $Ge_{15.0}$ $As_{21.0}$ $Ga_{1.0}$ $Se_{63.0}$ at. %//nominal as-batched $Ge_{21.0}$ $Sb_{10.0}$ $Se_{69.0}$ at. %: (**a**) SIF showing extraneous surface debris which is arrowed and (**b**) SIF core/cladding interface. Note that samples of this SIF (code: **F130RERC**) were demonstrated to exhibit lasing in [3].

using equipment configurations dependent on each sample geometry, as illustrated in Fig. 5. All PL measurements were carried out at room temperature (*21–23* °*C*), with excitation at 4.15 μm to stimulate $^2F_{5/2} \rightarrow {}^2F_{7/2}$ ground state absorption (red up-arrows in Fig. 1(c)) and the subsequent $^2F_{5/2} \leftarrow {}^2F_{7/2}$ emission of Ce^{3+} in each Ge-As-Ga-Se host geometry.

The open beam, 4.15 μm QCL (*quantum cascade laser*) pump (Fig. 5: item 9) was passed through a polarizer and then ¼ wave plate (Fig. 5: items 10, 11, respectively) to minimize pump reflections and unpolarized PL from the Ce^{3+}-doped glass sample affecting the QCL output. A 50/50 CaF_2 (*calcium-fluoride*) beam splitter feeding 50% of the power, originating from the QCL, to the thermal power meter (Fig. 5: items 12,13 respectively) was used to monitor continuously the 4.15 μm QCL power output during the measurement of PL from the Ce^{3+}-doped selenide chalcogenide glass samples.

The 4.15 μm QCL was electronically modulated at 12 Hz, using a 50% duty cycle, to modulate the Ce^{3+} PL output at the same frequency. This modulation achieved decoupling of the Ce^{3+} PL from any unmodulated thermal background noise of sample, surrounding equipment or personnel.

Equipment configurations (Fig. 5) to collect Ce^{3+} PL from the unstructured fibre, SIF, ground sample and bulk glass sample were as follows.

For the unstructured Ce-foil doped Ge-As-Ga-Se fiber, and the core// cladding = Ce-foil doped Ga-Se // Ge-Sb-Se SIF, the 4.15 μm QCL beam was focused into one end of the fiber (Fig. 5: items in 7(a)); the emitted Ce^{3+} PL, together with any unabsorbed 4.15 μm QCL light, were collected from the opposite fiber end. This equipment configuration is termed 'end-collection' in Fig. 5, inset **A**.

For the high surface area, ground sample, a length of the unstructured Ce-foil doped, Ge-As-Ga-Se fiber was ground by means of an agate mortar and pestle (*Fisher*), inside a glovebox (*MBraun, MB 150B-G*), under a dry nitrogen atmosphere *(< 0.6* ppm H_2O *and < 0.3* ppm O_2*)* to a particle diameter of $\sim \leq 100$ μm. The ground sample was then enclosed, whilst still inside the dry, oxygen-depleted glovebox atmosphere, in a hermetically sealed, in-house made, powder sample-holder, equipped with CaF_2 windows, (Fig. 5: item 7(b)). The ground sample was kept sealed from the ambient atmosphere to avoid oxidation and adsorption/absorption of water during the PL measurements. The 4.15 μm QCL beam was directed into the powder sample holder, while the resultant, light-diffused Ce^{3+} PL, and unabsorbed 4.15 μm QCL light were collected from the opposite side of the powder sample holder, as in Fig. 5, inset **B**.

For the bulk Ce-foil doped Ge-As-Ga-Se glass sample, a cuboid was cut, ground and polished from the original glass melt (Section 2.1.1) with three adjacent orthogonal sides (converging at a corner of the cuboid) polished to a 1 μm surface finish. The remaining faces were roughened with 120 grit sandpaper to reduce unwanted specular Fresnel reflection. The 4.15 μm QCL beam was focused into one polished face, as close to the edge between two of the polished faces as possible, of the bulk sample (Fig. 5: item 7(c)); the Ce^{3+} PL and reflected 4.15 μm QCL light were collected orthogonally, again as close to the edge between the launch face and collection face, as possible, in a 'side-collection' equipment configuration to minimize the optical path, and hence reabsorption, as illustrated in inset **C**, in Fig. 5.

An interchangeable optical filter (Fig. 5: item 3) was positioned in the optical circuit after the sample under measurement and before the monochromator, so as to block any unabsorbed or reflected 4.15 μm pump QCL light. In the same position, a long-pass filter, cut-on wavelength 4.203 μm, was used to transmit portions of the emission spectra at wavelengths longer than the 4.15 μm excitation wavelength, while, either a 3.80 μm band pass filter, or no filter, was used to transmit portions of the spectra at wavelengths shorter than the 4.15 μm excitation wavelength.

A monochromator (Fig. 5: item 2) was placed in the optical circuit just before the MIR detector (Fig. 5: item 1). The monochromator separated spatially the incoming broadband Ce^{3+} PL into its constituent wavelengths; it then directed the selected wavelengths to the monochromator exit where the MIR detector was positioned to measure the relative intensity at each wavelength selected by the monochromator.

Intensity measurements of the Ce^{3+} PL were aided with the use of a lock-in amplifier (Fig. 5, item 18); the modulation frequency of the Ce^{3+} PL was used as a reference signal for the lock-in amplifier, thus improving the signal-to-noise ratio of the detected PL intensity.

The PL emission lifetime 'τ_{rad}' and rise time 't_{rise}' were measured with the aid of a USB (Universal Serial Bus) oscilloscope (Fig. 5, item 16) and these were measured at a fixed, user-defined wavelength. During the switch OFF portion of the 50% duty cycle of the 4.15 μm QCL, the decaying Ce^{3+} PL emission intensity from the sample was recorded using the USB oscilloscope. Conversely, the increase in Ce^{3+} PL intensity was recorded during the ON portion of the 50% duty cycle. The repetitive nature of the electronic modulation of the pump source allowed the lifetime and rise time measurements to be averaged over several thousand iterations.

Note: the detection system response time for the rise and fall times of the 4.15 QCL source was measured to be < 1 μs; the rise time was taken as the time for the Ce^{3+} PL emissions to rise from 10% to 90% of the peak intensity, and PL lifetime data were fitted in MATLAB using the non-

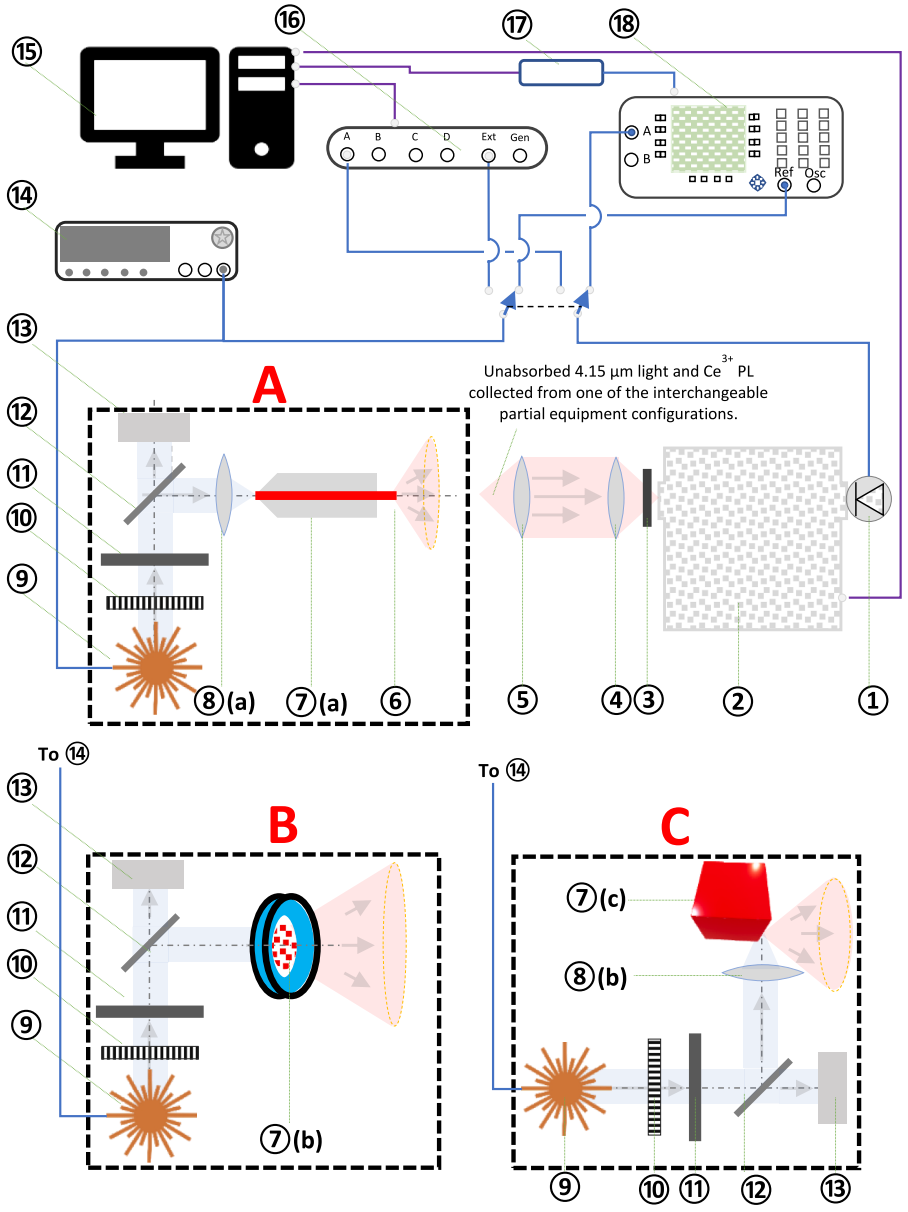

1) Mercury cadmium telluride detector (*Vigo Systems, PVI-4TE-6*).
2) Monochromator (*Spex Minimate*) with diffraction grating blazed at 6 µm. Purged with dry, atmosphere (H_2O & CO_2 *removed*).
3) Interchangeable optical filter:
   i. None
   ii. 3.80 µm bandpass filter (*Spectrogon, BP-3800-180nm*)
   iii. 4.203 µm long wave pass filter (*Northumbria Optical Coatings Ltd, SLWP-4203-001138*).
4) CaF_2 (*calcium fluoride*) lens, f = 40 mm (*Thorlabs, LA5370*) on XYZ translational stage.
5) Germanium lens, f = 12.5 mm (*Edmund Optics #89-607*) on XYZ translational stage.
6) Stainless steel 'V-groove' fiber holder.
7) Ce-doped chalcogenide glass sample:
   a) Single material fiber or SIF sample, with both ends cleaved.
   b) Powdered glass in sample holder fitted with two CaF_2 windows (*Crystran, CAFP20-1*).
   c) Cuboid shaped, polished bulk glass sample.
8) Focusing lens on XYZ translational stage:
   a) Aspheric lens, f = 5.95 mm (*Thorlabs, 390028-E*).
   b) Bi-convex CaF_2 lens, f = 15 mm (*Thorlabs, LB5766-E*).
9) 4.15 µm QCL laser (*Pranalytica 1101-42-CW-2500LH*).
10) Polarizer (*Thorlabs LPMIR050-MP2*).
11) ¼ wave plate (*Thorlabs WPLQ05M-4000*) on rotation mount.
12) 50/50 CaF_2 beam splitter (*Thorlabs, BSW520*) on kinematic mount.
13) Thermal power meter (*Thorlabs, C-Series S302C*).
14) Function generator (*GW Instek SFG-2104*).
15) Control and data acquisition computer.
16) USB oscilloscope (*Picoscope 5444b*).
17) National Instruments USB-6009 multifunction I/O.
18) Lock-in amplifier (*Ametek Signal Recovery, 7270 DSP*).

Fig. 5. Optical circuit equipment configurations to investigate PL emission spectra, PL lifetime and PL rise time of Ce-doped chalcogenide glass samples. Note the three interchangeable partial equipment configurations: inset **A:** configuration used for unstructured fiber (as-drawn, hence unannealed) and SIF (unannealed) samples, inset **B:** configuration used for the ground unstructured fiber (unannealed), and inset **C:** configuration used for polished, annealed bulk glass sample.

linear least squares method for a multi-term exponential function of the following form:

$$I(t) = \left(\sum_{j=1}^{n} A_j \times exp^{\left(\frac{-t}{\tau_j}\right)} \right) + Y_0 \quad (1)$$

where: 'n' is the number of exponential terms used to fit the empirical data; 'A_j' is the non-zero coefficient of each exponential term which expresses the fraction of the contribution of that term to the overall exponential process; 'τ_j' are the radiative lifetimes of each exponential term, and 'Y_0' is a constant relating to the signal-to-noise ratio of the detection system.

To obtain lifetime results (Fig. 7 and Table 1), data were fitted using Equation (1) to a single-term ($n = 1$), two-term ($n = 2$), and three-term ($n = 3$) exponential functions. The root mean square errors (RMSE) of each of these fittings were then compared to each other to evaluate the 'goodness-of-fit'. The fitting with both the lowest RMSE and lowest number of exponential terms, was then selected to avoid under-fitting or over-fitting. This was done to best fit the lifetime data, accounting for confounding factors such as sample geometry, pump power density and any inhomogeneities in the glass emission behavior [29,30], while at the same time avoiding unnecessary additional fitting terms.

The following subsections present the results of PL emission spectra, lifetimes and rise-time, respectively.

2.2.5.1. Results: Ce^{3+} PL emission spectra. The 4.15 µm QCL excitation scheme yielded broad Ce^{3+} PL emission between 3.40 and 5.80 µm wavelength, peaking around 4.60 µm, as shown in Fig. 6, attributed to the $^2F_{5/2} \leftarrow {}^2F_{7/2}$ emission transition (see Fig. 1(c)). Note that a portion of the emission spectrum: 3.90–4.40 µm as shown in Fig. 6, was

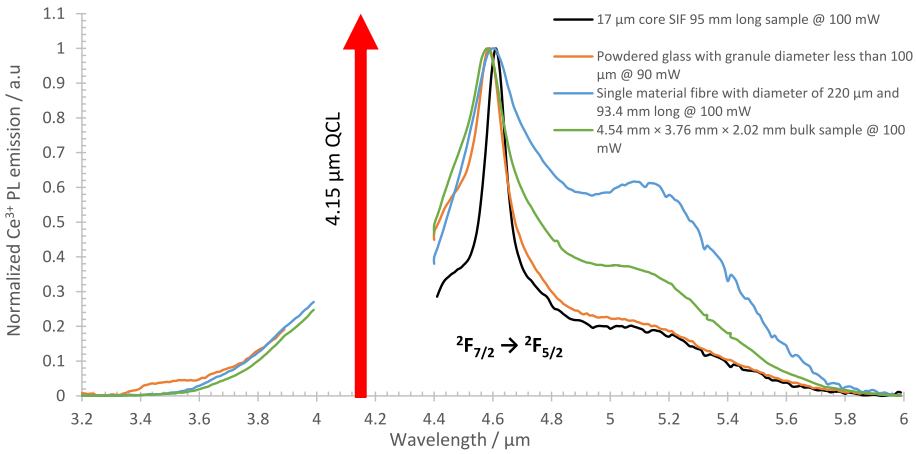

Fig. 6. Normalized Ce^{3+} PL emission spectra from unstructured glass fiber sample (as-drawn, so unannealed), SIF (as-drawn, so unannealed), sample, annealed bulk glass sample, and ground unstructured fiber (unannealed), annealed bulk glass sample, each with the nominal as-batched composition: 500 ppmw Ce foil doped $Ge_{15.0}$ $As_{21.0}$ $Ga_{1.0}$ $Se_{63.0}$ at. % composition, excited with a 4.15 μm QCL source. **Note**: a 4.203 μm long wave pass filter was used here for wavelengths greater than 4.15 μm while **no** filter was used here for wavelengths below 3.90 μm. Presented spectra are normalized at the peak intensity of Ce^{3+} PL emission for each sample geometry, and are uncorrected for the system spectral response.

purposefully omitted due to the presence of unabsorbed 4.150 μm QCL pump light. Additionally, spectra were normalized, within each sample geometry, to the individual peak Ce^{3+} PL intensity and were uncorrected for the system spectral response.

2.2.5.2. Results: Ce^{3+} PL lifetime and rise time. Fig. 7 shows the normalized Ce^{3+} PL emission lifetime 'τ_{rad}', and normalized Ce^{3+} PL rise time 't_{rise}', measured for each sample geometry, *viz.*: unstructured fiber (unannealed), SIF (unannealed), annealed bulk glass and ground unstructured fiber (unannealed). Note that all samples were from the same glass melt and so share the same nominal as-batched composition: 500 ppmw Ce-foil doped $Ge_{15.0}$ $As_{21.0}$ $Ga_{1.0}$ $Se_{63.0}$ atomic % (cf. SEM analysis of the SIF core was: $Ge_{16.2}$ $As_{20.0}$ $Ga_{0.9}$ $Se_{62.9}$ atomic %, see Section 2.2.4).

Both 'τ_{rad}' and 't_{rise}' measurements were carried out at each of 3.80 μm, 4.60 μm and 5.20 μm wavelengths and are shown in Fig. 7. 'τ_{rad}' (*best fitted to equation (1)*), and 't_{rise}' (10%–90% maximum PL) values are presented in Table 1.

Note that the lifetime and rise time results measured at 3.80 μm wavelength utilized a 3.80 μm band pass filter, while a 4.203 μm long pass filter was used for the longer wavelength measurements at 4.60 and 5.20 μm. In Table 1, the 'τ_{rad}' and 't_{rise}' at 3.80 μm and 5.20 μm of the ground glass sample, and at 3.80 μm for the SIF sample, are omitted due to the Ce^{3+} PL intensity being too weak to measure.

3. Discussion

3.1. Fabrication and optical characterization of fibers

In this paper, we have explained in more detail the fabrication and characterization of the selenide-chalcogenide glass SIF (*step-index fiber*), with a Ce^{3+} doped core, which was reported earlier to fiber lase beyond 5 μm wavelength [3]. The SEM analyzed SIF core//cladding compositions were (Section 2.2.4): $Ge_{16.2}$ $As_{20.0}$ $Ga_{0.9}$ $Se_{62.9}$ ± 0.5 at.% (cf. *nominal as-batched:* 500 ppmw Ce-foil doped *$Ge_{15.0}$ $As_{21.0}$ $Ga_{1.0}$ $Se_{63.0}$ at. %*)//$Ge_{21.5}$ $Sb_{11.2}$ $Se_{67.3}$ ± 0.5 at %, (cf. *nominal as-batched: $Ge_{21.0}$ $Sb_{10.0}$ $Se_{69.0}$ at. %*). The core glass composition was also found amenable to direct drawing to unstructured fiber, with relatively low optical loss (Fig. 3). These losses could in the future be reduced, by more stringent purification of chemical precursors *via* distillation [31,32]. Additionally, both the Ce-foil doped core and the undoped cladding selenide-chalcogenide glass compositions were sufficiently stable and thermally matched to undergo co-processing to fabricate the SIF without adversely changing the spectroscopic properties of the Ce-dopant (see Fig. 6) found in the bulk, as annealed glass: as-batched, 500 ppmw Ce-foil doped $Ge_{15.0}$ $As_{21.0}$ $Ga_{1.0}$ $Se_{63.0}$ at. % (*code: M259REZQT*).

3.2. Photoluminescence characterization of Ce^{3+}-doped samples

The Ce-dopant was the most electropositive element during glass melting of the 500 ppmw Ce-foil doped $Ge_{15.0}$ $As_{21.0}$ $Ga_{1.0}$ $Se_{63.0}$ at. % (*code: M259REZQT*, Section 2.1.1) and hence the most reactive species present for scavenging both adventitious anionic impurities like hydroxide and oxide and, through hydration and hydrolysis, impurity water. Thus, in effect the cerium dopant was an effective 'getter', chemically reacting with these unwanted impurities during glass melting. This implies that unwanted cerium III oxide and hydroxide represents a portion of Ce^{3+} sites whose first excited state would be depopulated by the locally high phonon energy. Moreover, the Ce-dopant could potentially have been oxidized further to assume its tetravalent oxidation state 'Ce^{4+}', for example in the form CeO_2 or $CeSe_2$. 'Ce^{4+}' comprises an inner electronic configuration of [Xe], with no available '4f' electrons for 4f ⇌ 4f intra-electronic transition and therefore no electronic mechanism for MIR absorption or MIR PL production. Thus again, a proportion of the doped in cerium would be removed from contributing to MIR PL or fibre lasing.

The Ce-doped samples, no matter the different sample geometries, consistently yielded a broad Ce^{3+} PL emission spectrum as shown in Fig. 6. To explain the breadth of the PL band, notably: (i) a portion of this emission spectrum could have exhibited intra-up-conversion between Stark levels inside the one manifold of the first excited state, resulting in Ce^{3+} PL emissions at wavelengths as short as 3.40 μm, we suggest that this was phonon-assisted up- and down-conversion and/or (ii) a population of electrons resided in a second Stark level of the ground state; this occupation at room temperature – christened a 'hot transition' in ref. [7] for Ce^{3+} doped oxide hosts, hence opening the possibility of excitation from this upper ground state to the excited state manifold. This process is marked by the dotted red arrow in Fig. 1(c).

In fact, the emission of anti-Stokes photoluminescence is a well-known phenomenon, which forms not only the basis for optical refrigeration, but also has been consistently observed in ytterbium (III) doped oxide glass fiber [33].

The shorter wavelength (so higher photon energy, longer arrows in Fig. 1(c)) emissions could only have originated from the uppermost Stark level of the excited state $^2F_{7/2}$ manifold, as illustrated in Fig. 1(c). Conversely, the longest wavelength Ce^{3+} PL emissions (lowest photon energy, shorter arrows in Fig. 1(c)) could only have originated from the lowest Stark level of the upper $^2F_{7/2}$ manifold but may have dropped either to the uppermost Stark level of the ground state or to second lowest Stark level of the ground state, rather than the lowest Stark level of the ground state [7].

Now, considering the 4.15 μm excitation wavelength, then electrons excited into the $^2F_{7/2}$ manifold may have undergone an additional energy transfer, entailing phonon-assisted both upward and downward

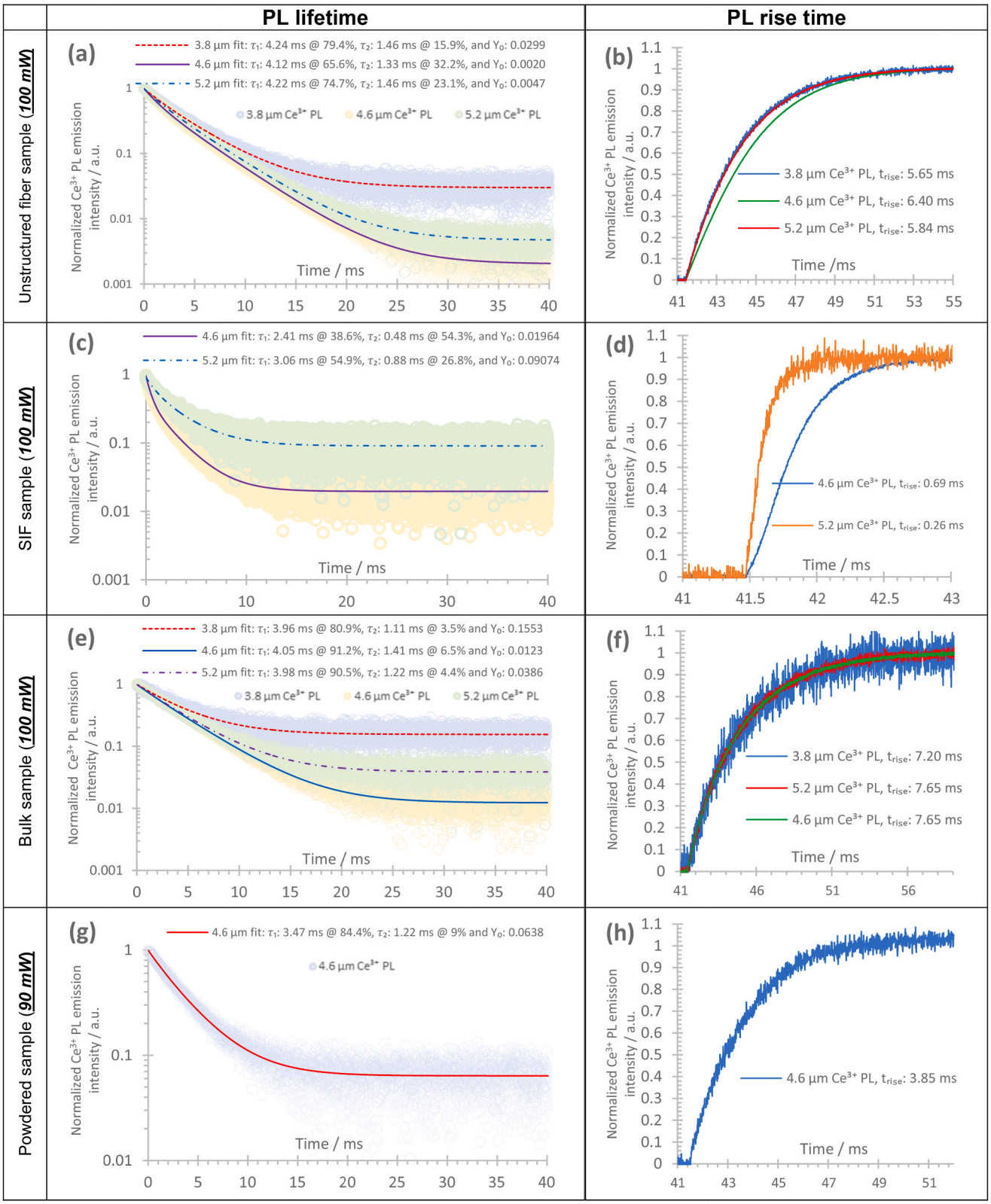

Fig. 7. For unstructured fibre, SIF, bulk glass and ground unstructured fibre, made from the same glass melt which was each with the nominal as-batched composition: 500 ppmw Ce foil doped $Ge_{15.0}$ $As_{21.0}$ $Ga_{1.0}$ $Se_{63.0}$ at. % composition, these are the normalized Ce^{3+} PL lifetime (**scatter plot**) then fitted with the exponential decay function from eqn. (1) (**smooth red plot**), along with Ce^{3+} PL rise time (**blue plots**) at wavelengths of 3.8 μm, 4.6 μm and 5.2 μm, respectively, pumped with 4.15 μm QCL modulated at 12 Hz. Figures **(a)–(b)**: unstructured fiber (as-drawn, so unannealed) of diameter 220 ± 5 μm and 93.4 mm long; Figures **(c)–(d)**: SIF (as-drawn, so unannealed) sample of 17 μm core diameter and 95 mm long; Figures **(e)–(f)**: bulk glass (annealed) sample 4.54 mm × 3.76 mm × 2.02 mm, and Figure **(g)–(h):** ground unstructured fiber (unannealed) sample of particle size ~ ≤ 100 μm diameter. Please see Table 1 for collation of PL lifetime and rise time results.

Table 1
Summary of Ce^{3+} PL lifetime and rise time measurements shown in Fig. 7.

Sample type and dimensions	Measurement wavelength/ μm	PL lifetime coefficients					Rise time 10%–90%
		A_1	τ_1/ ms	A_2	τ_2/ ms	Y_0	τ_{rise}/ms
Unstructured fiber (un-annealed) diameter of 220 μm *and 93.*4 mm *long.*	3.80	0.794	**4.24**	0.159	1.46	0.02992	5.65
	4.60	0.656	**4.12**	0.322	1.33	0.00203	6.40
	5.20	0.747	**4.23**	0.231	1.46	0.00469	5.84
SIF (un-annealed) core diameter of 17 μm, *and 95.*0 mm *long.*	4.60	0.386	**2.41**	0.543	**0.48**	0.01964	0.69
	5.20	0.549	**3.06**	0.268	0.88	0.09074	0.26
*Bulk glass (annealed and polished) 4.*54 mm × *3.*76 mm × *2.*02 mm.	3.80	0.809	**3.96**	0.035	1.11	0.15530	7.20
	4.60	0.912	**4.05**	0.065	1.41	0.01230	7.65
	5.20	0.905	**3.98**	0.044	1.22	0.03861	7.65
Powdered glass (from unstructured fiber, un-annealed) varying granule size ≤ 100 μm *in diameter.*	4.60	0.844	**3.47**	0.090	1.22	0.06379	3.85

Note: *all samples are from the same glass melt and so share the same nominal* $Ge_{15.0}$ $As_{21.0}$ $Ga_{1.0}$ $Se_{63.0}$ *atomic % composition doped with 500 ppmw Ce foil.*

transitions, to redistribute themselves between its upper and lower bounds to account for the very broad Ce^{3+} PL emission spectrum observed and the 1130 cm^{-1} width of the excited state $^2F_{7/2}$ manifold.

Considering Fig. 6, the PL emission spectrum produced by the unstructured, unannealed fiber showed signs of reabsorption resulting in an increase of PL intensity at longer wavelengths, around ~5.10 μm, when compared to emission spectra of the other sample geometries. In contrast, both the ground glass (from grinding the unstructured fiber) and SIF samples produced an emission spectrum which was similar to each other and due in both cases to the shorter emission pathlength. The emission pathlength of the ground glass was restricted by the particle-size of <~100 μm both of the particles giving a lack of propensity for reabsorption. Similarly in the SIF, Ce^{3+} emission in all directions from the doped core would have meant some PL would be guided in the undoped cladding lowering the probability of reabsorption but still suffering the underlying linear loss of core and cladding.

Unilaterally, the SIF sample exhibited a more prominent peak emission at 4.61 μm which, moreover was slightly red-shifted and these differences are unexplained at present. It was expected that the annealed bulk glass sample, due to its innate short pathlength, would resemble more clearly the ground sample, however this was not the case and the annealed bulk glass seemed to suffer reabsorption, This latter may have been due to artefact from the optical set-up like unwanted internal reflections inadvertently increasing the optical pathlength of the emission. But, it should also be remembered that another difference between the Ce^{3+}ions located in the SIF core compared to in the bulk glass was one of annealing; thus the SIF was unannealed and the bulk glass host was annealed. Annealing can affect the number of defect states in a glass and this in turn may affect the PL character; more experiments are required to understand if this is so.

Both the unstructured fiber and the bulk glass samples exhibited little variation in their respective PL lifetime and rise time results over the measurement wavelengths, as shown in Fig. 7 and Table 1.

Conversely, the PL lifetime results for the SIF sample exhibited a notable difference between the 4.60 μm (τ_1: 2.41 ms; (τ_2: was 0.48 ms) ms; and 5.20 μm (τ_1 was 3.06 ms; τ_2 was 0.88 ms) measurement wavelengths. Similarly, the PL rise time measurements for the SIF sample also exhibited a difference between measurement wavelengths: at 4.60 μm, τ_{rise} = 0.69 ms and at 5.20 μm, τ_{rise} = 0.26 ms. Additionally, the rise time of the SIF sample (sub-unity ms) differed significantly from the other sample types (~4–7 ms) at these two wavelengths. These differences for the SIF sample indicated some other influence, possibly due to differences in stress/strain due to the fabrication process, glass host composition, and/or effective pump energy density, within the sample geometry.

Considering also the pronounced peak at 4.61 μm observed in the PL emission spectrum obtained from the SIF sample (*see Fig. 6), it was postulated that stimulated emission at 4.*60 μm *was influencing the measured PL lifetime and rise time at 4.*60 μm *while the 5.*20 μm *measurement wavelength was unaffected due to a lack of stimulated emission there.*

Considering both the unstructured fiber and the bulk glass samples, the consistency in their respective PL lifetimes and rise times indicated a uniform behavior for the ground state absorption followed by the upward and downward redistribution within the $^2F_{7/2}$ manifold, and subsequent Ce^{3+} PL emission over the measurement wavelengths. However, this behavior deviates at higher power density when considering the results from the SIF sample in the postulated presence of stimulated emission.

We are embarking on cryogenic measurements to illuminate more clearly whether in these Ce^{3+}-doped very low phonon energy glass hosts there is a Stark level structure in the ground state, as observed in the high phonon energy oxide glass hosts [7] and will report later on these results.

4. Conclusions

We have demonstrated the fabrication and characterization of a chalcogenide glass SIF (step-index fiber), comprising a core glass composition of nominal as-batched: 500 ppmw Ce-foil doped $Ge_{15.0}$ $As_{21.0}$ $Ga_{1.0}$ $Se_{63.0}$ at. % and cladding glass composition: of nominal as-batched: $Ge_{21.0}$ $Sb_{10.0}$ $Se_{69.0}$ atomic %. Using in-band pumping at 4.15 μm, very wide, broadband PL (photoluminescence) has been observed from the doped in Ce^{3+} cations between 3.40 and 5.80 μm, attributed to the $^2F_{5/2} \leftarrow {}^2F_{7/2}$ electronic emission transition. PL emission spectra, PL lifetimes, and PL rise times were measured in Ce-foil doped unstructured fiber (as-drawn so unannealed) SIF with 17 μm diameter core, an annealed bulk glass sample and the same unstructured fiber glass sample ground up. PL lifetimes up to 4.24 ms were measured, while PL rise times 't_{rise}' measurements ranged widely between the different sample geometries between 0.26 ms and 7.65 ms.

Funding

'Thematic Studentship' funded by the UK Engineering and Physical Sciences Research Council (EPSRC), funding grant ref. EP/N50970X/1; PhD funding from EPSRC DTG funding grant ref. EP/N50970X/1; EPRSC

through Projects: (i) COOL (COld-cOntainer processing for Long-wavelength mid-infrared fiberoptics, EP/P013708/1 and SHAPE (Ceramic SHaping: extrusion of glAss Preforms for new fibres in hEalthcare), EP/T010762/1.

Declaration of competing interest

The authors declare that they have no known competing financial interests or personal relationships that could have appeared to influence the work reported in this paper.

Data availability

Data will be made available on request.

Acknowledgements

Joel Nunes acknowledges with gratitude his 'Thematic Studentship' funded by the UK Engineering and Physical Sciences Research Council (EPSRC), funding (grant ref. EP/N50970X/1). Richard Crane thanks EPSRC for his DTG funding (grant ref. EP/N50970X/1). David Furniss was supported by EPRSC through Projects (i) COOL (COld-cOntainer processing for Long-wavelength mid-infrared fiberoptics, (EP/P013708/1) and SHAPE (Ceramic SHaping: extrusion of glAss Preforms for new fibres in hEalthcare) (EP/T010762/1).

The Authors are grateful for the use of the Woollam IR-VASE Mark II ellipsometer at the School of Science and Technology, Department of Physics and Mathematics, Nottingham Trent University, Clifton Campus in Nottingham, UK.

References

[1] L.B. Shaw, B. Cole, P.A. Thielen, J.S. Sanghera, I.D. Aggarwal, Mid-wave IR and long-wave IR laser potential of rare-earth doped chalcogenide glass fiber, IEEE J. Quant. Electron. 37 (9) (2001) 1127–1137, https://doi.org/10.1109/3.945317.

[2] A.B. Seddon, Z.Q. Tang, D. Furniss, S. Sujecki, T.M. Benson, Progress in rare-earth-doped mid-infrared fiber lasers, Opt Express 18 (25) (2010) 26704–26719, https://doi.org/10.1364/OE.18.026704.

[3] J.J. Nunes, Ł. Sojka, R.W. Crane, D. Furniss, Z.Q. Tang, D. Mabwa, B. Xiao, T. M. Benson, M. Farries, N. Kalfagiannis, E. Barney, S. Phang, A.B. Seddon, S. Sujecki, Room temperature mid-infrared fiber lasing beyond 5 μm in chalcogenide glass small-core step index fiber, Opt Lett. 46 (15) (2021) 3504–3507, https://doi.org/10.1364/OL.430891.

[4] P. Fjodorow, M.P. Frolov, S.O. Leonov, B.I. Denker, B.I. Galagan, S.E. Sverchkov, V. V. Koltashev, V.G. Plotnichenko, M.V. Sukhanov, A.P. Velmuzhov, Mid-infrared laser performance of Ce^{3+}-doped selenide glass, Opt Express 29 (17) (2021) 27674–27682, https://doi.org/10.1364/OE.433828.

[5] S. Cotton, Lanthanide and Actinide Chemistry, John Wiley & Sons, Ltd, West Sussex, UK, 2006.

[6] F.M.A. Sroor, F.T. Edelmann, Lanthanides: tetravalent inorganic, in: R.A. Scott (Ed.), Encyclopedia of Inorganic and Bioinorganic Chemistry, John Wiley & Sons, Ltd, Chichester, UK, 2012, p. eibc2033, https://doi.org/10.1002/9781119951438.eibc2033.

[7] M.J. Weber, Optical spectra of Ce^{3+} and Ce^{3+}-sensitized fluorescence in $YAlO_3$, J. Appl. Phys. 44 (7) (1973) 3205–3208, https://doi.org/10.1063/1.1662735.

[8] G.H. Dieke, H.M. Crosswhite, The spectra of the doubly and triply ionized rare earths, Appl. Opt. 2 (7) (1963) 675, https://doi.org/10.1364/AO.2.000675.

[9] A.P. Kozlova, V.M. Kasimova, O.A. Buzanov, K. Chernenko, K. Klementiev, V. Pankratov, Luminescence and vacuum ultraviolet excitation spectroscopy of cerium doped $Gd_3Ga_3Al_2O_{12}$ single crystalline scintillators under synchrotron radiation excitations, Results Phys. 16 (2020), 103002, https://doi.org/10.1016/j.rinp.2020.103002.

[10] A. Herrmann, H.A. Othman, A.A. Assadi, M. Tiegel, S. Kuhn, C. Rüssel, Spectroscopic properties of cerium-doped aluminosilicate glasses, Opt. Mater. Express 5 (4) (2015) 720, https://doi.org/10.1364/OME.5.000720.

[11] V.B. Pawade, S.J. Dhoble, Spin–orbit splitting difference and Stokes shift in $cerium^{3+}$-activated aluminate phosphors, Spectrosc. Lett. 46 (7) (2013) 472–475, https://doi.org/10.1080/00387010.2012.731025.

[12] G. Bellisola, C. Sorio, Infrared spectroscopy and microscopy in cancer research and diagnosis, Am. J. Cancer Res. 2 (1) (2012).

[13] J.S. Sanghera, L. Brandon Shaw, I.D. Aggarwal, Chalcogenide glass-fiber-based mid-ir sources and applications, IEEE J. Sel. Top. Quant. Electron. 15 (1) (2009) 114–119, https://doi.org/10.1109/JSTQE.2008.2010245.

[14] B. Bureau, C. Boussard-Plédel, S. Cui, R. Chahal, M.-L. Anne, V. Nazabal, O. Sire, O. Loréal, P. Lucas, V. Monbet, Chalcogenide optical fibers for mid-infrared sensing, Opt. Eng. 53 (2) (2014), 027101, https://doi.org/10.1117/1.OE.53.2.027101.

[15] A.B. Seddon, Mid-infrared (IR) - a hot topic: the potential for using mid-IR light for non-invasive early detection of skin cancer in vivo, Phys. Status Solidi B 250 (5) (2013) 1020–1027, https://doi.org/10.1002/pssb.201248524.

[16] E. Roeder, Extrusion of glass, J. Non-Cryst. Solids 5 (5) (1971) 377–388, https://doi.org/10.1016/0022-3093(71)90039-1.

[17] S.D. Savage, C.A. Miller, D. Furniss, A.B. Seddon, Extrusion of chalcogenide glass preforms and drawing to multimode optical fibers, J. Non-Cryst. Solids 354 (29) (2008) 3418–3427, https://doi.org/10.1016/j.jnoncrysol.2008.01.032.

[18] M. Suzuki, T. Kato, S. Watabe, Rod in Tube Method of Forming a Fiber Preform, with Maintaining a Gas Supply until after an End Is Stretched, US6425270B1, 1998.

[19] C. Strutynski, C. Strutynski, J. Picot-Clémente, A. Lemiere, P. Froidevaux, F. Désévédavy, G. Gadret, J.-C. Jules, B. Kibler, F. Smektala, Fabrication and characterization of step-index tellurite fibers with varying numerical aperture for near- and mid-infrared nonlinear optics, J. Opt. Soc. Am. B 33 (11) (2016) D12, https://doi.org/10.1364/JOSAB.33.000D12.

[20] J. Troles, Y. Niu, C. Duverger-Arfuso, F. Smektala, L. Brilland, V. Nazabal, V. Moizan, F. Desevedavy, P. Houizot, Synthesis and characterization of chalcogenide glasses from the system Ga–Ge–Sb–S and preparation of a single-mode fiber at 1.55μm, Mater. Res. Bull. 43 (4) (2008) 976–982, https://doi.org/10.1016/j.materresbull.2007.04.029.

[21] Z. Tang, D. Furniss, M. Fay, H. Sakr, L. Sójka, N. Neate, N. Weston, S. Sujecki, T. M. Benson, A.B. Seddon, Mid-infrared photoluminescence in small-core fiber of praseodymium-ion doped selenide-based chalcogenide glass, Opt. Mater. Express 5 (4) (2015) 870, https://doi.org/10.1364/OME.5.000870.

[22] Z. Tang, V.S. Shiryaev, D. Furniss, L. Sojka, S. Sujecki, T.M. Benson, A.B. Seddon, M.F. Churbanov, Low loss Ge-As-Se chalcogenide glass fiber, fabricated using extruded preform, for mid-infrared photonics, Opt. Mater. Express 5 (8) (2015) 1722, https://doi.org/10.1364/OME.5.001722.

[23] W.A. King, A.G. Clare, W.C. LaCourse, Laboratory preparation of highly pure As_2Se_3 glass, J. Non-Cryst. Solids 181 (3) (1995) 231–237, https://doi.org/10.1016/S0022-3093(94)00512-5.

[24] T. Schweizer, Rare-Earth-Doped Gallium Lanthanum Sulphide Glasses for Mid-infrared Fibre Lasers, University of Southampton, Southampton, 1998.

[25] A.B. Seddon, D. Furniss, Z.Q. Tang, Ł. Sojka, T.M. Benson, R. Caspary, S. Sujecki, True mid-infrared Pr^{3+} absorption cross-section in a selenide-chalcogenide host-glass, in: 2016 18th International Conference on Transparent Optical Networks, ICTON), Trento, Italy, 2016, pp. 1–6, https://doi.org/10.1109/ICTON.2016.7550709.

[26] P. Sourková, P. Sourková, B. Frumarova, M. Frumar, P. Nemec, M. Kincl, V. Nazabal, V. Moizan, J.-L. Doualan, R. Moncorge, Spectroscopy of infrared transitions of Pr^{3+} ions in Ga–Ge–Sb–Se glasses, J. Lumin. 129 (10) (2009) 1148–1153, https://doi.org/10.1016/j.jlumin.2009.05.009.

[27] A. White, H.J. Williams, J.H. Wernick, R.C. Sherwood, Observation of a possible large crystalline Stark splitting in metallic Ce: $LaAl_2$f, Phys. Rev. E 131 (3) (1963) 1039–1042, https://doi.org/10.1103/PhysRev.131.1039.

[28] R.G. Goodrich, G.E. Everett, Electron spin resonance in cerium metal, Phys. Rev. E 141 (2) (1966) 541–547, https://doi.org/10.1103/PhysRev.141.541.

[29] Z. Tang, L. Sojka, D. Furniss, J. Nunes, H. Sakr, E. Barney, S. Sujecki, T.M. Benson, A.B. Seddon, Comparative study of praseodymium additives in active selenide chalcogenide optical fibers, Opt. Mater. Express 8 (12) (2018) 3910, https://doi.org/10.1364/OME.8.003910.

[30] H. Przybylińska, C.-G. Ma, M.G. Brik, A. Kamińska, P. Sybilski, A. Wittlin, M. Berkowski, Yu Zorenko, V. Gorbenko, H. Wrzesinski, A. Suchocki, Electronic structure of Ce^{3+} multicenters in yttrium aluminum garnets, Appl. Phys. Lett. 102 (24) (2013), 241112, https://doi.org/10.1063/1.4812190.

[31] M. Meneghetti, C. Caillaud, R. Chahal, J. Troles, Purification of Ge-As-Se ternary glasses for the development of high quality microstructured optical fibers, J. Non-Cryst. Solids 503 (504) (2019) 84–88, https://doi.org/10.1016/j.jnoncrysol.2018.09.028.

[32] V.S. Shiryaev, J.-L. Adam, X.H. Zhang, C. Boussard-Plédel, J. Lucas, M. F. Churbanov, Infrared fibers based on Te–As–Se glass system with low optical losses, J. Non-Cryst. Solids 336 (2) (2004) 113–119, https://doi.org/10.1016/j.jnoncrysol.2004.01.006.

[33] X. Xia, A. Pant, A.S. Ganas, F. Jelezko, P.J. Pauzauskie, Quantum point defects for solid-state laser refrigeration advanced materials, Adv. Mater. 33 (2021) 1–27, 1905406.